

Stephen M. Goodnick • Anatoli Korkin
Robert Nemanich
Editors

Semiconductor Nanotechnology

Advances in Information and Energy
Processing and Storage

 Springer

Chapter 8

Wave Vision



Vladimir P. Yakubov

Abstract The basic applications of radio waves are communication and radiolocation. In the proposed chapter, another application of radio waves is considered – radio wave tomography – which is based on penetration of radio waves into opaque media and the extraction of information about the three-dimensional internal structure of objects. The theory of extracting useful information in this case is solving inverse problems using aperture synthesis with focusing. The efficiency of this approach is illustrated by the numerous examples.

8.1 Review of Existing Approaches

In this chapter we present development of wave tomography methods as a means of remote nondestructive testing, diagnostics of the internal structure of semitransparent media, and reconstruction of the shapes of opaque objects based on methods of radiolocation. The word tomography derives from two Greek words: $\tau\omicron\mu\omicron\varsigma$, a layer, and $\gamma\rho\alpha\phi\epsilon\iota\omega$, to write. Thus, tomography means literally “to write a layer,” i.e., to investigate a structure layer-by-layer. The difference between tomography and other diagnostic methods is that information from the same test element is recorded in multiple integral projections, i.e., many times from different angles relative to the embedded inhomogeneities.

It has been over 50 years now since researchers in this field learned how to “clear up” these projections and recover the structure of inhomogeneities layer-by-layer. For the most part, this became possible, thanks to the development of new computational methods and computer technologies. At the present time, computed tomography is rightfully considered as an “absolute” diagnostic technique in medicine. Radio wave tomography is similar to X-ray and magnetic resonance imaging, but it is associated with electromagnetic radiation in the radio wave range. In this case, the wavelength of the radiation used is comparable to the characteristic size of the

V. P. Yakubov (✉)

Radio Physics Department, Tomsk State University, Tomsk, Russia
e-mail: yvlp@mail.tsu.ru

inhomogeneities, so that the diffraction effects and effects of multiple interactions are of great importance. For that reason, this form of tomography is sometimes called diffraction tomography. Without dwelling on all the different methods and approaches of diffraction tomography [1–33] that are currently available, let us focus instead on active location (detection) wave tomography, which is of vital importance, e.g., for security systems.

Radio wave systems are preferable in the development of contactless detection devices for a variety of reasons. In the first place, radio waves are practically harmless to human health. This is their crucial difference from ionizing X-rays. Second, the potential range of application of these systems is quite wide: in crowded public places, in special-forces raids for detection and tracking of people hiding behind walls, detection of injured persons after emergency events, etc. There is also a great demand for contactless and computer-aided systems for quality control in building construction, timber processing, and other industries.

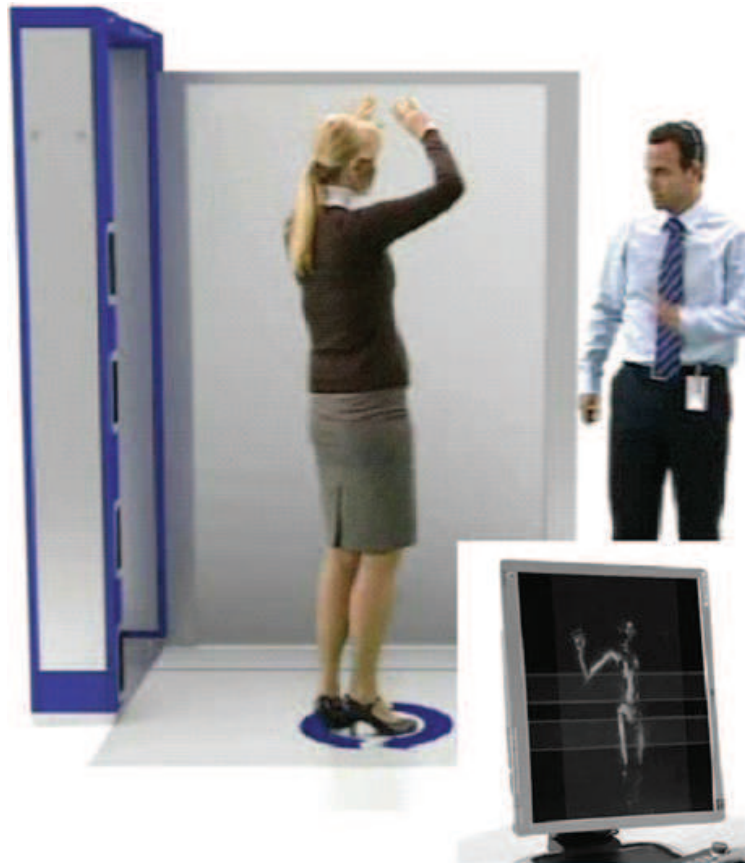
The variety of physical processes involved in radio wave detection, taking place in natural and simulated complex environments and involving complex objects, underlies the complexity of the mathematical descriptions of such processes and the urgency of solutions of the tomography problem as well.

Figures 8.1 and 8.2 show the known microwave passenger inspection systems. The screening of one person in this way takes 10–30 s, and the resolution obtained is

Fig. 8.1 The model of SafeScout 100 Scanner



Fig. 8.2 The model of Smiths Heimann



no better than 1 cm. The complexity of this system, substantial costs, and low resolution are its main disadvantages.

The use of ultra-wideband (UWB) systems and signals is considered to be the most promising approach from the standpoint of applications. The development of a radio-detection UWB tomograph requires the solution of a number of problems. Available commercial radio-detection include the Israeli scanner Raptor-1600 (Fig. 8.3), which is able to monitor the movement of large objects, e.g., a person moving behind a wall, and the Russian radio wave UWB scanner “RADIOVISION” (Fig. 8.4) which operates in real time at a speed of 10 fps.

As we see the radio wave systems already exist. However, this does not exhaust all of the currently available possibilities. The development of an optimal antenna array configuration is, of necessity, the first step in this process. This development would include the relative placement of the receiving and transmitting antennas and a determination of their minimum number required for tomographic imaging. The solution of this problem is one of the objectives of ongoing research. It includes determination of the optimal sequence of radar measurements to provide the required data digitization in a short period of time. Moreover, considerable attention must be paid to the development of fast algorithms for real-time 3D image restoration of scanned objects based on radio sounding data.

The antenna array optimization problem alluded to above also arises from the need to minimize the number of antennas in order to reduce antenna array costs



Fig. 8.3 The model of Raptor-1600 Scanner

Fig. 8.4 The model of
RADIOVISION



while holding the number of artifacts to a minimum. From the latter half of the twentieth century onward, several methods of antenna array optimization for radio astronomy and aircraft detection have been developed. The antenna array optimization problem is a natural outgrowth of the problem referred to as antenna array design with minimum redundancy. Accordingly, the antennas should be positioned in such a way as to effectively solve the problems that arise.

Over the past few decades, a great deal of research has been conducted, and field-proven results have been obtained in the far-field zone of narrowband antenna arrays. However, a subject of particular interest to the authors is antenna arrays for ultra-wideband radiation, which are designed to characterize objects located in the array focusing area. So far, this issue has not been investigated as there has not been any urgency to research the near-field zone of antenna arrays. In this context, the near-field zone is considered as the region of space at a distance on the order of the dimensions of the array. In other words, this refers to the Fresnel diffraction zone.

The next development of tomogram methods is the construction of images of hidden objects by using wave projections. In this context, the two following requirements come to the forefront: adequate restoration accuracy and real-time performance of the system. There is some contradiction here, which is formulated as “Fast is not always best.” Reconstruction should be performed in real-time mode, for instance, in a minute. The task is complicated when it is impossible to obtain complete measurement data. This situation arises when the scanning is performed non-equidistantly, in motion, or when the object to be detected is hidden inside a building or under clothing near the body.

A phase information record is provided by radio-frequency holography, in which the result of interference of the background wave and the object wave is recorded. The wave projection record is in fact a radio-hologram record. From general considerations, it is clear that large aperture synthesis is the preferable method for post-processing these projections since it provides the highest spatial resolution. Currently there are a large number of variations of this method under continuous development [33].

Electromagnetic radiation interacts with electrophysical inhomogeneities in the propagation medium. In contrast to electromagnetic radiation, acoustic radiation interacts mainly with density inhomogeneities. In this context, using ultrasound for tomography of an inhomogeneous medium provides a wide range of additional possibilities, particularly for determining the type of material that the hidden items are made of.

The current state of research on remote ultrasonic sounding has revealed that practically all of these methods are based on contact measurements. The reason is that ultrasound is strongly attenuated by air. The only ultrasonic sounding system (sonar vision) which is actually efficient in air is bat echolocation. Some insects also generate ultrasound, but rather for scaring and masking from bats. The practical use of ultrasound in a liquid medium or through immersion liquids (e.g., in metal working, medicine, etc.) is well known. Preliminary studies hold out the hope for the effective use of ultrasound for purposes of near-field tomography in air, and our main focus areas include:

- Physical and mathematical models of an image reconstruction system for an inhomogeneous medium based on tomographic processing of multi-angle projection records of scattered radio wave and acoustic radiation
- Key elements of the modeling system
- Subsystems and elements of a multi-angle measuring tool
- Experimental measurement techniques
- Evaluation of potential and actual performance-based specifications for a detecting tomograph with different measurement and sounding schemes

The wide practical application of UWB tomography is still limited, on the one hand, by considerable engineering problems in generating and receiving UWB radiation and by complications, on the other hand, that arise when describing and interpreting simultaneously manifested physical phenomena of the interaction of the radiation with matter. These phenomena include multiple scattering, diffraction, wave interference, and absorption of ultra-wide-bandwidth radiation from arbitrarily placed and randomly oriented inhomogeneities of different size. A multitude of combinations of these effects hinders solution of the direct problem – a description of the integral effects of the wave disturbance. Solution of the inverse problem and reconstruction of the distribution of inhomogeneities in the tested volume are problematic under such conditions in any event. Researchers have no choice but to solve such inverse problems. These tasks are generally referred as ill-posed problems, which require the use of regularizing algorithms. The most stable inverse problems are the simplest ones, which account for the dominant mechanisms of the interaction of waves with the propagation media and make it possible to single out (identify) such mechanisms.

Inverse problems are of crucial importance for applications such as sounding the optically opaque media. When radio-frequency radiation penetrates into such a medium, analysis of the transmitted and scattered fields makes it possible to reconstruct its internal structure. This internal structure consists in the spatial distribution of the permittivity. Steep permittivity gradients are typical for interfaces and for immersed objects. A typical example is searching for hidden archaeological graves, underground cables, or antipersonnel landmines and ground covers as well as detection and identification of prohibited items in stowed luggage and in hand-carried items. Problems of this sort are not simple, but a great number of efficient solutions have been developed for them based on radiation focusing. With regard to a radiopaque object, radiation hardly penetrates it, so the solution of the inverse problem in this case reduces to reconstructing the shape of the object on the basis of an analysis of scattered (reflected) radiation.

Interesting directions for the future development of radiotomography include techniques for implementing incoherent radiation and low-frequency magnetic fields. The spectrum of radio tomography applications is extremely wide.

8.2 Focusing Wave

Focusing is the main tool that allows you to visualize probed heterogeneities using both pulsed and monochromatic radiation. Let us elucidate the essence of the proposed solution in the particular case of a homogeneous background medium in the single scattering approximation

$$E(\boldsymbol{\rho}_0, f) = k_1^2 \iiint_{V_1} \Delta\varepsilon(\boldsymbol{\rho}_1, z_1) G_0^2(\boldsymbol{\rho}_1 - \boldsymbol{\rho}_0, z_1) d^2\boldsymbol{\rho}_1 dz_1. \quad (8.1)$$

Here $k_1 = k = 2\pi f/c$ is the wave number corresponding to the background medium. Green's function is written in this case as a spherical wave field:

$$G_0(\boldsymbol{\rho}_1 - \boldsymbol{\rho}_0, z_1) = \exp\left\{ik\sqrt{(\boldsymbol{\rho}_1 - \boldsymbol{\rho}_0)^2 + z_1^2}\right\}/4\pi\sqrt{(\boldsymbol{\rho}_1 - \boldsymbol{\rho}_0)^2 + z_1^2}.$$

If we differentiate Eq. (8.1), we can write

$$\frac{d}{dk} \left\{ \frac{E(\boldsymbol{\rho}_0, f)}{k^2} \right\} = \int \int_{V_1} \int \Delta\varepsilon(\boldsymbol{\rho}_1, z_1) G_2(\boldsymbol{\rho}_1 - \boldsymbol{\rho}_0, z_1) d^2\boldsymbol{\rho}_1 dz_1,$$

where

$$G_2(\boldsymbol{\rho}_1 - \boldsymbol{\rho}_0, z_1) \equiv \exp\left\{i2k\sqrt{(\boldsymbol{\rho}_1 - \boldsymbol{\rho}_0)^2 + z_1^2}\right\}/4\pi\sqrt{(\boldsymbol{\rho}_1 - \boldsymbol{\rho}_0)^2 + z_1^2}.$$

This function admits a plane-wave decomposition of the spectrum (Weyl's formula):

$$G_2(\boldsymbol{\rho}_1 - \boldsymbol{\rho}_0, z_1) = \frac{i}{(2\pi)^2} \int \int \frac{\exp\{i(\boldsymbol{\kappa}_\perp(\boldsymbol{\rho}_1 - \boldsymbol{\rho}_0) + \boldsymbol{\kappa}_z z_1)\}}{2\boldsymbol{\kappa}_z} (d^2\boldsymbol{\kappa}_\perp),$$

where $\boldsymbol{\kappa}_z = \sqrt{(2k)^2 - \boldsymbol{\kappa}_\perp^2}$. Taking this representation into account, we can write

$$\begin{aligned} E_1(\boldsymbol{\rho}_\perp, f) &\equiv \int \int \exp\{i\mathbf{u}_\perp \boldsymbol{\rho}\} \frac{d}{dk} \left\{ \frac{E(\boldsymbol{\rho}_0, f)}{k^2} \right\} d^2\boldsymbol{\rho}_0 = \\ &\iint \int_{V_1} \Delta\varepsilon(\boldsymbol{\rho}_1, z_1) \frac{\exp\{i(\boldsymbol{\rho}_\perp + \mathbf{u}_z z_1)\}}{2i\mathbf{u}_z} d^2\boldsymbol{\rho}_1 dz_1, \end{aligned} \quad (8.2)$$

where $\mathbf{u}_z = \sqrt{(2k)^2 - \mathbf{u}_\perp^2}$. This expression implies that the spatial frequency spectrum of the inhomogeneities coincides with the obtained expression for $E_1(\mathbf{u}_\perp, f)$ to within a factor:

$$\begin{aligned}\Delta\varepsilon(\mathbf{u}_\perp, \mathbf{u}_z) &\equiv \iiint_{V_1} \Delta\varepsilon(\boldsymbol{\rho}_1, z_1) \exp\{i(\mathbf{u}_\perp \boldsymbol{\rho}_1 + \mathbf{u}_z z_1)\} d^2 \boldsymbol{\rho}_1 dz_1 \\ &= 2i\mathbf{u}_z E_1(\mathbf{u}_\perp, f).\end{aligned}\quad (8.3)$$

In the final count, the three-dimensional inverse Fourier transform remains to be performed to recover the spatial distribution of the inhomogeneities. There is only one calculational peculiarity here if expression (8.2) is used, and that is the need to transform from time frequencies f to the corresponding spatial frequencies

$$u_z = \sqrt{(2k)^2 - \mathbf{u}_\perp^2} = \sqrt{(4\pi f/c)^2 - \mathbf{u}_\perp^2},$$

which is realized by interpolation. Expression (8.3) realizes the idea of the focusing method at all distances.

Here and below, the problem of large aperture synthesis with radiation focusing is called radio wave tomosynthesis. Equation (8.3) in this case is a generalization of the Stolt method [28, 33], and it takes into account the difference between the functions $G_0(\boldsymbol{\rho}_1 - \boldsymbol{\rho}_0, z_1)$ and $G_2(\boldsymbol{\rho}_1 - \boldsymbol{\rho}_0, z_1)$. It should be noted that this substitution acts as a selection of the window function and does not affect the focusing procedure.

The proposed method is applicable in the case of a multilayer medium. It suffices, for this purpose, to replace the exponential factor $\exp(iu_z z_1)$ by the combined factor

$$\exp\left\{i \sum_j u_{zj} z_j + i u_z z_1\right\},$$

which accounts for the phase difference for all previous layers with depths z_j and refractive indices n_j . The normal projection of the wave number in each of the layers is calculated as

$$u_{zj} \equiv \sqrt{(2kn_j)^2 - \mathbf{u}_\perp^2}.$$

As an experimental test of this approach, a model medium was constructed from three foam-concrete blocks with equal depth of 10 cm (Fig. 8.5a). A thin test layer made from five aluminum foil strips with equal width of 2 cm (Fig. 8.5b) was placed between the second and third blocks. The aluminum test layer is indicated by an arrow. The measured refractive index of the foam-concrete was $n = 1.44$. A radio image of the test layer obtained by the proposed method is shown in Fig. 8.5b as a gray-scale plot. Sounding was performed using UWB pulses with a pulse duration of 200 ps.

The radio image reproduces the actual size and positions of the aluminum strips with a resolution of at least 2 cm. If the background medium is inhomogeneous, the resolution will be a bit worse.

The fundamental idea of radio wave tomosynthesis is to develop a focusing effect as a result of partial wave interference. The connection between radio wave

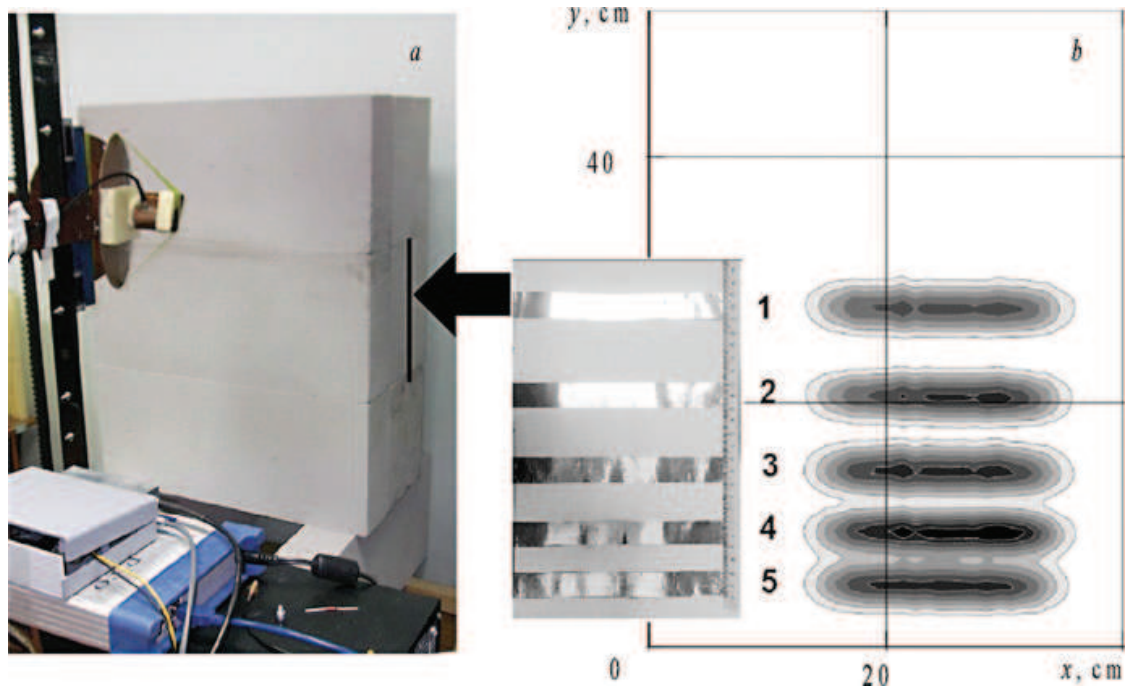


Fig. 8.5 Experiment to validate the group focusing approach: (a) a wall made of foam, concrete blocks; (b) test object inside the wall and its radio image

tomosynthesis and multidimensional matched filtering and other methods has been pointed out.

It has been demonstrated that the focusing effect, which is the basis of wave tomography, significantly reduces the effect of multiple interactions and amplifies the role of the dominant mechanisms of the radiation-matter interaction.

The emphasis has been upon location sounding, where the radiation and receiving points are located in the same half-space. Many of the algorithms proposed for the solution of the inverse problem reduce to fast algorithms and admit of real-time operation.

Most of the solutions considered have been borne out by numerical simulation and real experiments.

8.3 Experimental Examples

8.3.1 Antennas and Signals

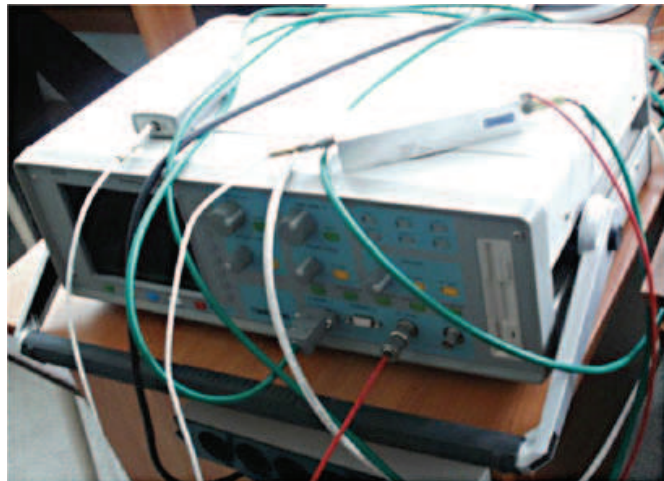
The basic setup for UWB radio wave sounding includes a scanner, an XY positioner (Fig. 8.6), a scanner control unit, a TMR8140 stroboscopic oscilloscope (Fig. 8.7), a personal computer, and a transceiver module (Fig. 8.8).

The transceiver module is worthy of note. The original design of the UWB antenna is implemented in this device (Fig. 8.9). The antenna is constructed two electric antennas (a TEM horn and an asymmetrical dipole) and a magnetic antenna



Fig. 8.6 Scanner for UWB measurements

Fig. 8.7 TMR8140
stroboscopic oscilloscope
and bipolar pulse generator
with a duration of 0.1 ns



of spiral shape. The overlap of the near-field zones of these unlike (electric and magnetic) antennas makes it possible to considerably reduce the presence of reactive fields and extend the bandwidth as a result.

The displacement of the antenna phase center for the frequency spectrum does not exceed its diameter. The design of the antenna was developed by Associate Professor J. I. Buyanov.

Fig. 8.8 Transceiver module



Fig. 8.9 UWB antennas of snail type

The frequency characteristic of the smallest of the antennas is shown in Fig. 8.10. The bandwidth of this antenna is 1–18 GHz. The voltage standing wave ratio (VSWR), which is a specification used to rate antennas, does not exceed 2.

The directivity diagram of the antenna, by virtue of its small size, is quite wide in both the azimuthal and the elevation plane (30–70°). Directivity diagrams (DDs) of the antenna, measured at two frequencies (3 GHz and 9 GHz), are shown in Fig. 8.11.

Signals with durations of 100, 200, and 1500 ps were analyzed for radio sounding. Equipment from TRIM, Ltd. – Research and Production Enterprise (St. Petersburg, Russia) (TRIM Ultrawideband Measurement Systems) – was used to generate and receive the UWB signals. The pulse repetition rate of the strobe was 100 kHz. Analysis of signal forms and spectra (Fig. 8.12) revealed that pulses with durations of 100 and 200 ps were most relevant for radio tomography. These signals in particular should provide proper spatial resolution, and their spectra are well-matched to the chosen design of the transceiver antenna.

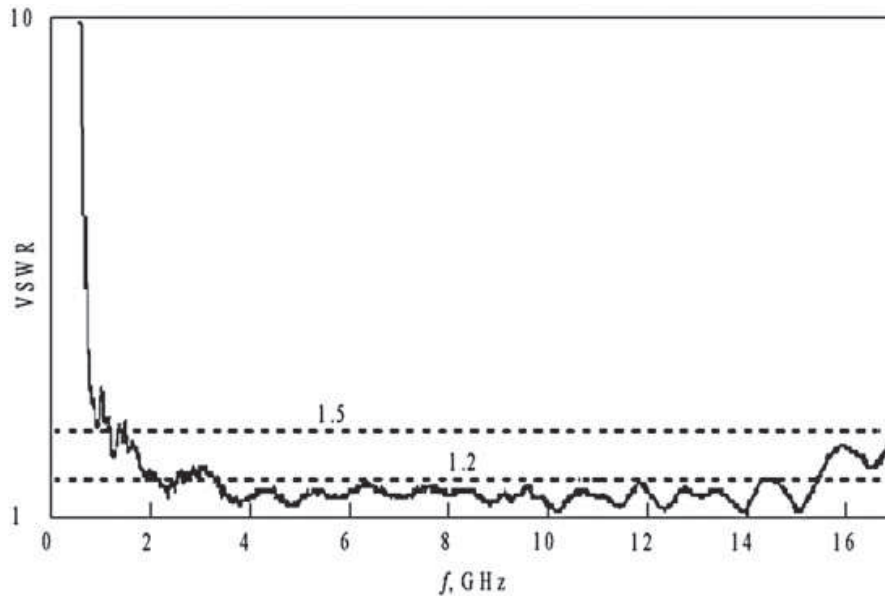


Fig. 8.10 VSWR frequency dependence of snail-type antennas

A typical signal with a duration of 100 ps, reflected from the test object, is shown in Fig. 8.13. The signal is of indented form, and the central peak is delayed by the travel time from the object to the antenna module.

Figure 8.14 displays a sample raster image of recorded signals from scanning the test object. The line-by-line rasters presented here are set one above another. In this case, horizontal flyback of the scanner starts immediately after direct scanning of the previous line.

This considerably shortens the scanning time. It is important that the characteristic diffraction hyperbola, which indicates the localization of the object, is distinctly visible at every step.

The scanner control unit contains a USB-to-COM converter based on the FTDI 245BM chip. This makes it possible to transform low-current USB command signals into eight binary output signals, which after being routed through matching amplifiers are directed to the stepper motor control of a two-coordinate scanner. There are four windings in each stepper motor, where the current in each of them assigns the motor state. The control unit makes it possible to position the scanner antenna module along two axes independently. In general, the experimental setup allows the transceiver antenna module to be repositioned within an 84×84 cm square region in the plane with an accuracy of 2 mm and a speed of up to 3 cm/s.

Employing monostatic radiometry methods to solve problems of tomography in most cases supposes the use of a single antenna for both reception and transmission in a way that facilitates more accurate reconstruction of the radio wave image of the tested object, all other things being equal. In UWB tomography, the use of a single antenna is complicated by technical difficulties associated with isolation of the transmitting and receiving antenna paths. It proved to be impossible to find suitable directional couplers providing isolation of not less than 30 dB in the UW frequency band. Development of a fast UWB switch is another independent task.

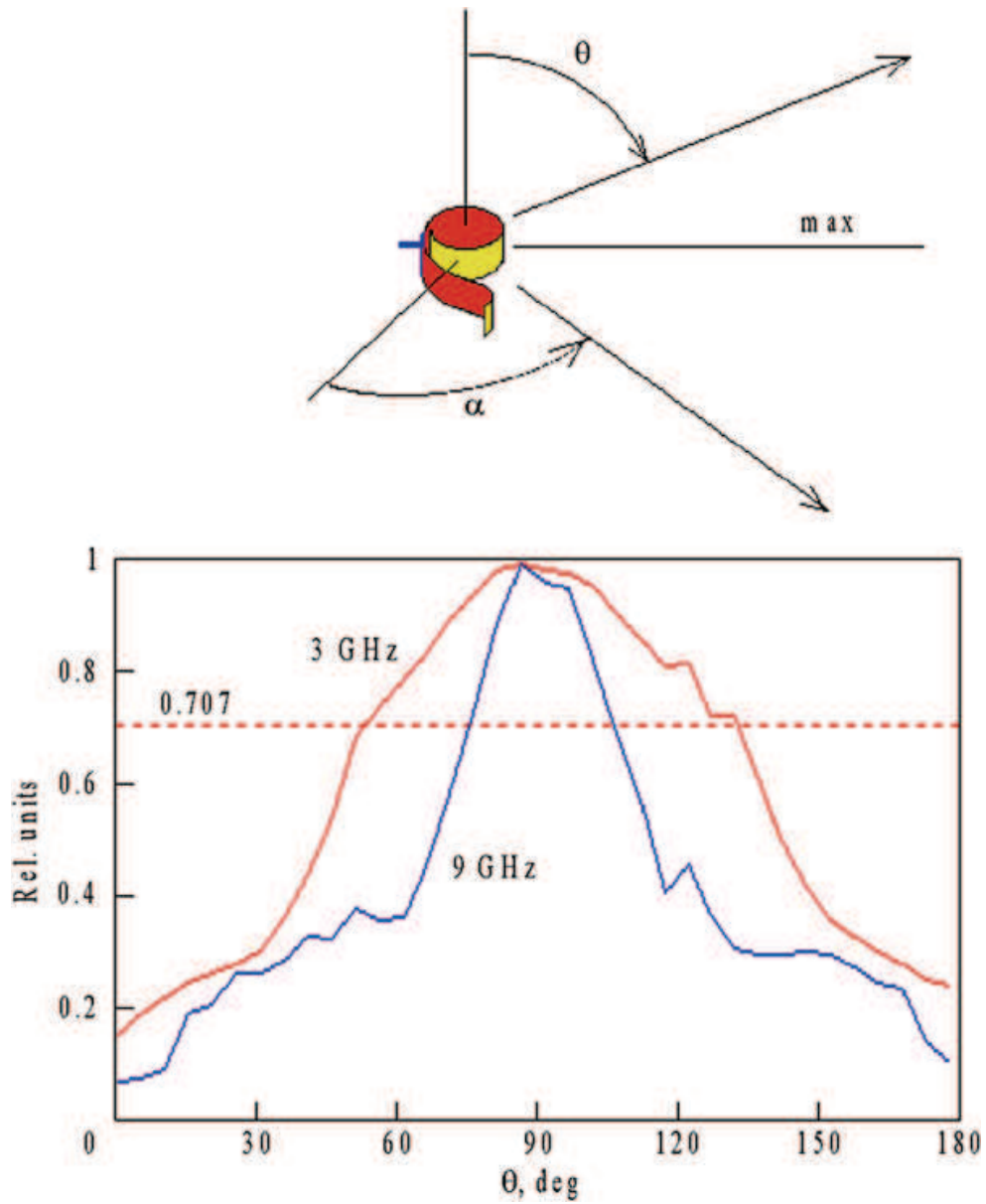


Fig. 8.11 Azimuthal DD of a snail-type antenna

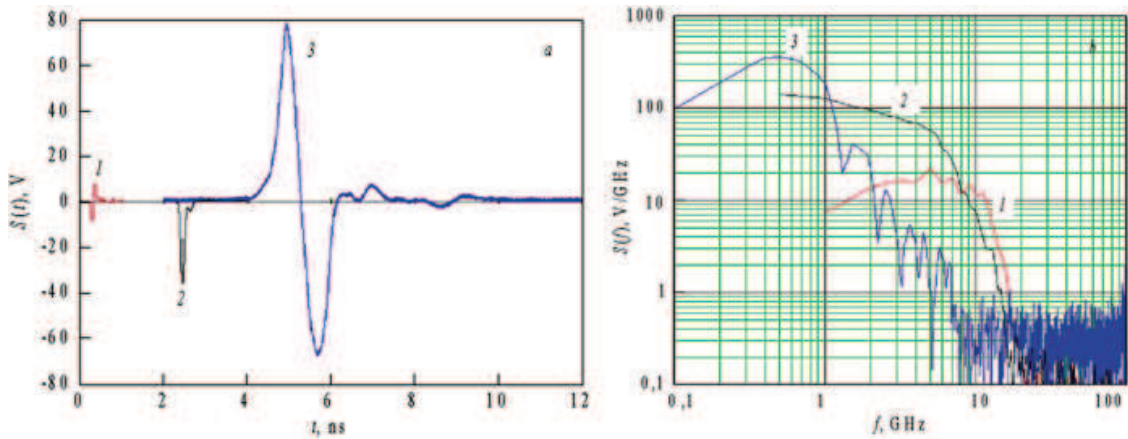


Fig. 8.12 UWB pulses of different duration (a) used for sounding and their spectra (b): curve 1–100 ps; curve 2–200 ps; curve 3–1500 ps

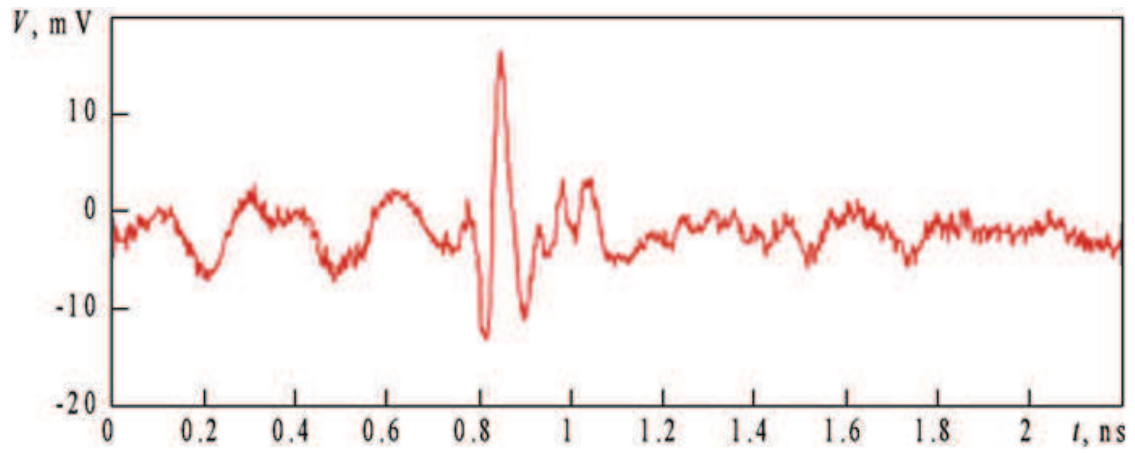


Fig. 8.13 A UWB signal reflected from the test object

Fig. 8.14 Radio wave scanning image of tested section

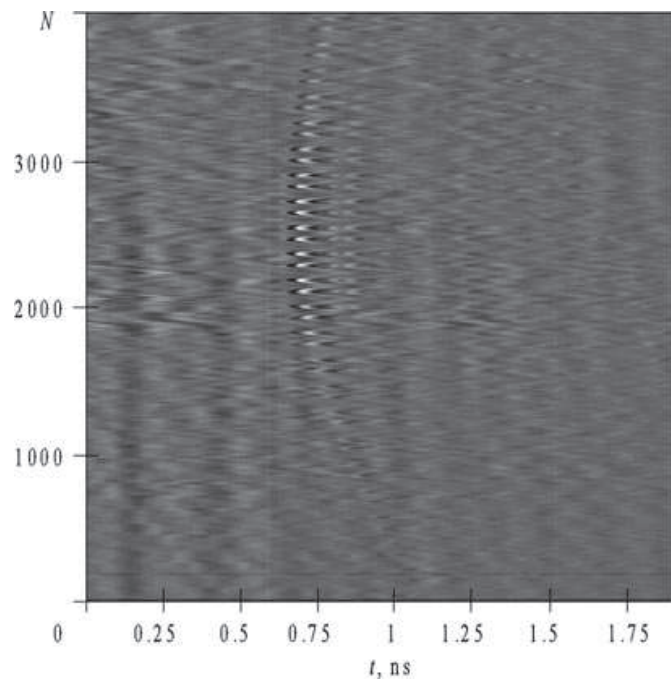


Fig. 8.15 Plastic suitcase (a) and case contents (b)

It was experimentally determined that the antennas must be separated by a distance of not less than 20 cm to get isolation of 25–30 dB between the receiving and transmitting antennas; however, this is unacceptable in UWB tomography.

To increase the decoupling from the transmitting antenna to the receiving antenna, a metallic screen was used, whose shape and geometric dimensions were determined experimentally. It turned out that an acceptable result was achieved when the screen had a shape close to that of an ellipse with major and minor semi-axes of 9 and 5 cm, respectively. A photograph of the assembly of antennas with screen is shown in Fig. 8.9.

8.3.2 *Different Various Objects and Their Radio Image*

UWB tomography is especially effective for luggage inspection. A plastic suitcase with a plastic gun and a bottle of water inside it is shown in Fig. 8.15. Figure 8.16 presents the tomography of this scene.

The experimental setup described above (see Fig. 8.7) was used for tomosynthesis of images of hidden objects in media with metallic inclusions. First off, a wooden carrying box reinforced with metal bands was sounded (Fig. 8.17). The dimensions of the box were $47 \times 41 \times 19$ cm.

A metal-coated stepped triangle was placed in the box. Each step of the triangle was 5 cm in length. There was a 2×2 cm square hole in the center of the triangle (Fig. 8.18).

Scanning was performed by moving the transceiver antenna module in the Oxz plane with a step of 1 cm. The scanning area had dimensions 60×50 cm. The test

Fig. 8.16 UWB tomogram of case contents





Fig. 8.17 UWB scanner and carrying box

object was fastened to the bottom of the box at a range of 39 cm, as shown in Fig. 8.18. Range is reckoned in the OZ direction from the transceiver antenna module.

As a result of UWB scanning and data processing, a 3D tomogram of the contents of the box was obtained (Fig. 8.19). Cross section (*a*), which corresponds to the upper cover of the box at a range of 18.5 cm, reveals the reinforcing tape along the perimeter of the cover and a metal handle in the center of the cover.

Wooden latches at the back side of the front of the box can be observed in cross section (*b*), which corresponds to a range of 21.5 cm. Cross section (*c*) corresponds to a range of 22.5 cm. The same inhomogeneities are visible in it. The test object, a triangle with a central hole, is visible in cross section (*d*) corresponding to a range of 39 cm.

Cross section (*e*) at a range of 42 cm corresponds to the back of the box. The back of the box and a radio shadow from the test object are clearly visible in cross sections (*e*) and (*f*). A radio shadow appears since the test object is metal-coated and therefore radiopaque.



Fig. 8.18 Test object inside the box

According to the results of the experiment, it may be concluded that implementation of tomosynthesis algorithms makes it possible to tune out interference caused by echo signals reflected from the reinforcing elements. The obtained tomogram allowed us to determine the depth of the test object with an accuracy better than 0.5 cm and visualize its shape as well.

Next, let us consider experimental results of visualization of an object placed in an open metal container. A metal safe with dimensions $64 \times 48 \times 41$ cm was used for this purpose (see Fig. 8.20). The door of the safe was taken off its hinges. Figure 8.21 shows the safe from behind.

On completion of scanning, a tomogram was obtained which showed the distribution of inhomogeneities in the tested space. Radio images of cross sections at different ranges are presented in Fig. 8.22. Figure 8.22a presents a cross section corresponding to the upper cover of the safe at a range of 18.5 cm. The front frame of the safe stands out distinctly in the tomogram. The cross section corresponding to a range of 19 cm is shown in Fig. 8.22b. This tomogram demonstrates the sunken frame used to hang the door. The cross section corresponding to a range of 53 cm is shown in Fig. 8.22c. In this tomogram, the test object with central hole is distinctly visible. The cross section at a range of 62 cm is shown in Fig. 8.22d. This cross section images the back wall of the safe.

Based on the experimental results, it may be concluded that implementing tomosynthesis algorithms makes it possible to tune out interference caused by echo signals reflected from the walls and bottom of the metal container. The obtained

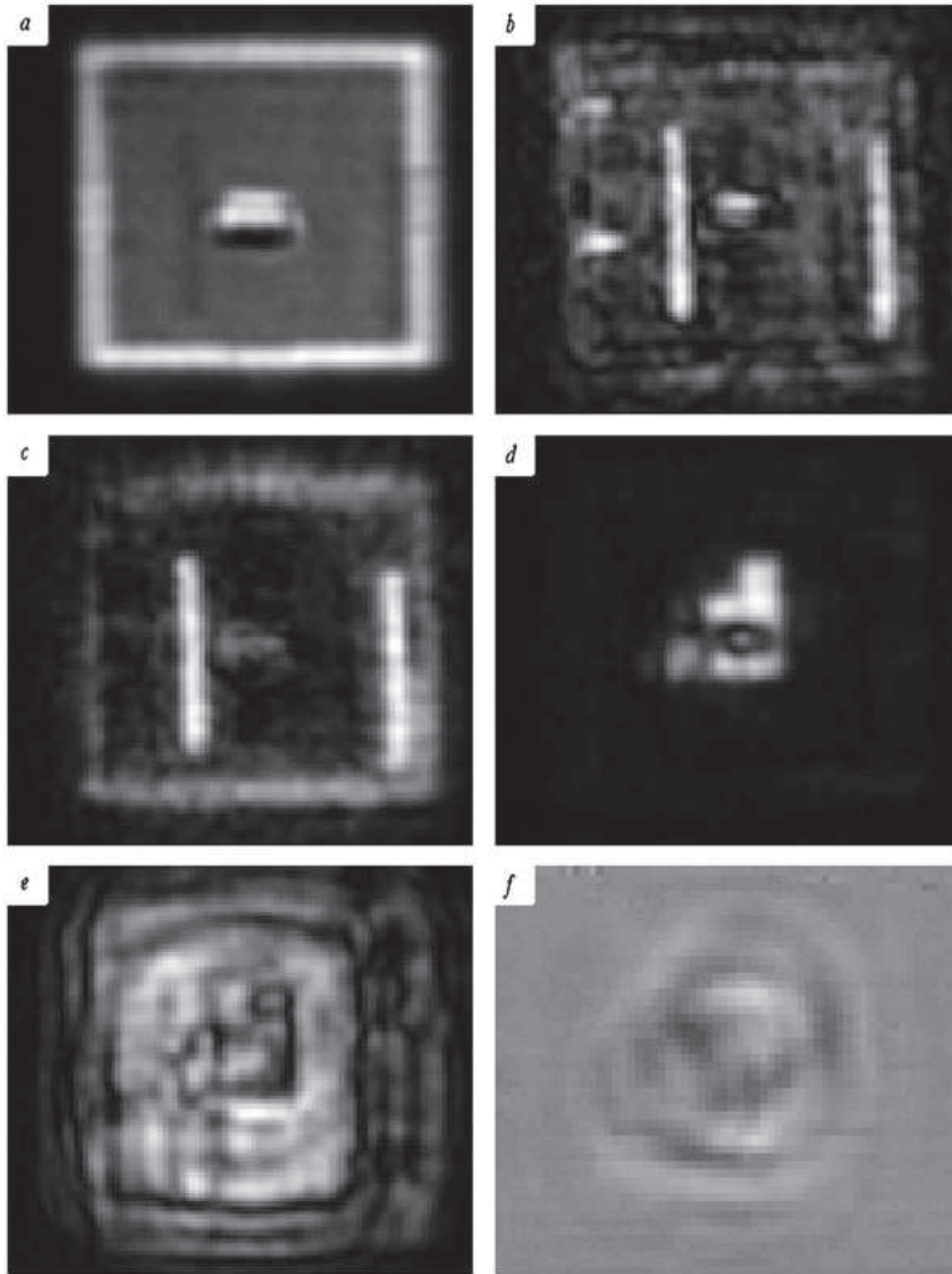


Fig. 8.19 Radio wave tomogram of a wooden box (with a metal band along its edge) and its contents

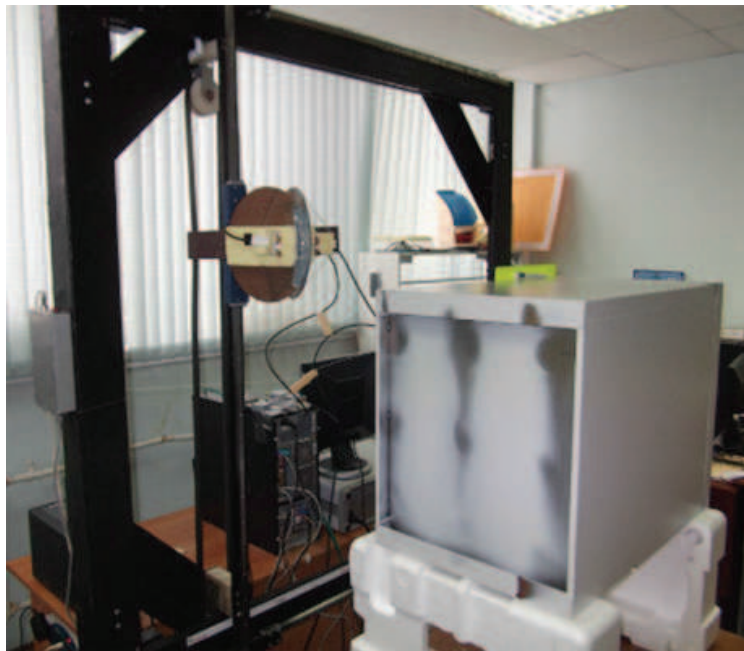
tomogram allows the depth of test object to be determined and the shape of the object to be visualized as well.

Searching big trucks in order to prevent the transportation of prohibited articles such as weapons, explosives, etc. is a major problem at access control points (ACPs). There are special-purpose X-ray detectors for that purpose, but it is not possible to equip all of the critical ACPs owing to the high cost of the equipment. A relatively cheaper radio wave system for detecting and visualizing hidden objects can be implemented to search dump trucks and similar vehicles. It is depicted in Fig. 8.23.

Fig. 8.20 Test object inside the metal safe



Fig. 8.21 Back view of the safe



The system is basically a clocked array of UWB antennas, which are switched by electromechanical switching devices. When a truck moves through this system at low speed, it will be possible to sound the truck body in order to detect hidden objects under the load (soil, sand, etc.). A prototype of this system is shown in Fig. 8.4.

The best possible resolution in the radio range can be obtained in the millimeter frequency range. This is the range where practically all American radio scanner prototypes work. It is an important fact that the resolution in this band is usually sufficient to recognize fine details of an object, while the penetration remains on a reasonable level.

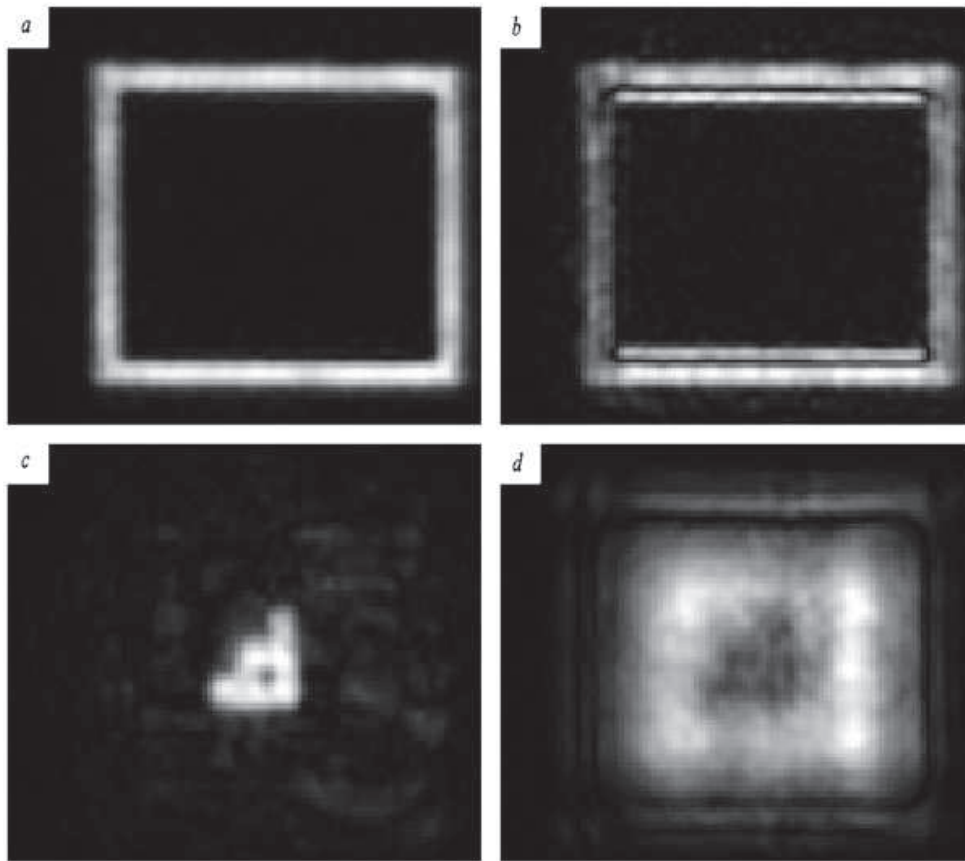


Fig. 8.22 Ultrasonic tomogram of a metallic box and its contents



Fig. 8.23 Advanced system for detecting and visualizing hidden objects at ACPs

8.3.3 Ultrasonic Vision

Electromagnetic radiation interacts with electrophysical inhomogeneities in the propagation medium. In contrast to electromagnetic radiation, acoustic radiation interacts mainly with density contrasts in the sounding medium. In this context, using ultrasound in the tomography of inhomogeneous media provides additional opportunities, in particular for detecting the type of material that the hidden objects are made of. Integration of radio and acoustic sounding provides opportunities, e.g., for the detection of explosives.

A search on remote ultrasonic sounding techniques reveals that most industrial methods are based on contact measurements. The principal reason for this is that ultrasound attenuation in air is quite high. Ultrasound is used in Parktronic systems for car parking and for control of industrial robots. The ultrasound system (echolocation) used by bats is perhaps the only ultrasonic ranging system actually effective in air (see Fig. 8.24).

Some insects also use ultrasound, but rather for active jamming of bats' sounding. There is no doubt in the efficiency of ultrasound for sounding in liquids and through immersion liquids. This applies in the fields of industrial metal working, medicine, and submarine echolocation. In nature this also pertains to dolphins and fish. However, ultrasound can be efficiently used for tomography in air in safety systems and in nondestructive testing. If the object is radiopaque, radiation can hardly penetrate it, and only acoustic radiation will allow the recovery of its internal structure.

From a mathematical perspective, acoustic wave propagation is similar to the propagation of electromagnetic waves. Both electromagnetic and acoustic waves are described by wave equations, and both give rise to reflection, scattering, and diffraction effects when the wave interacts with inhomogeneities in the medium. In this respect, all of the mathematical methods and results elaborated in previous chapters are applicable for ultrasound.

The simplest setup for our experiments in ultrasound tomography is shown in Fig. 8.25. Standard piezoceramic transmitters and ultrasound receivers with a



Fig. 8.24 Bats are effective ultrasonic stations in air

Fig. 8.25 Experimental setup for ultrasonic tomography

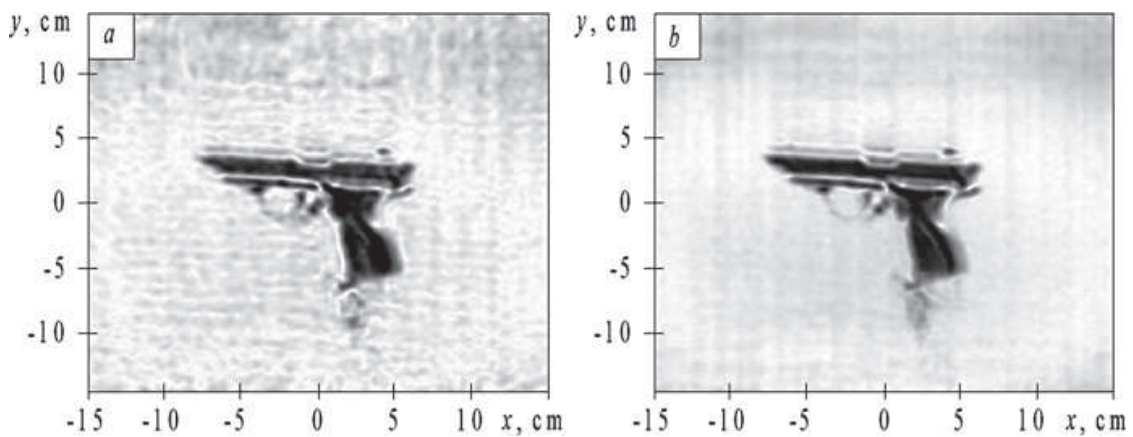


Fig. 8.26 Recovered image of the object (tomogram): at a frequency of 40 kHz (a), within the frequency band 37–43 kHz (b)

resonant frequency of 40 kHz are set on an x-y recorder, and a computer sound card can be employed as a signal generator and receiver. A Creative Audigy SE PCI SB0570 sound card enables signal generation and recording with a sample rate up to 96 kHz. An MA40S4R ultrasonic transmitter was used as well as an EM9767 electret microphone. The object of sounding (a toy gun) was placed at a certain distance from the transmitter. Scanning was performed through a simple computer-aided controller.

The restored image of the test object is presented in Fig. 8.26. The image of a gun can be clearly distinguished in the result of single-frequency sounding; however, there are minor artifacts. The number of artifacts was markedly decreased when the

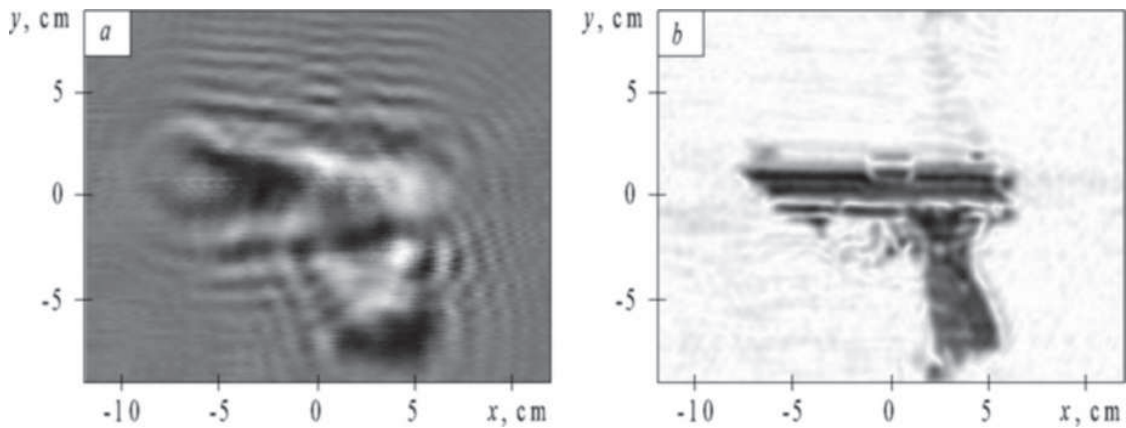


Fig. 8.27 Plastic gun in air at a distance of 10 cm: measured data (a) and result of focusing (b)

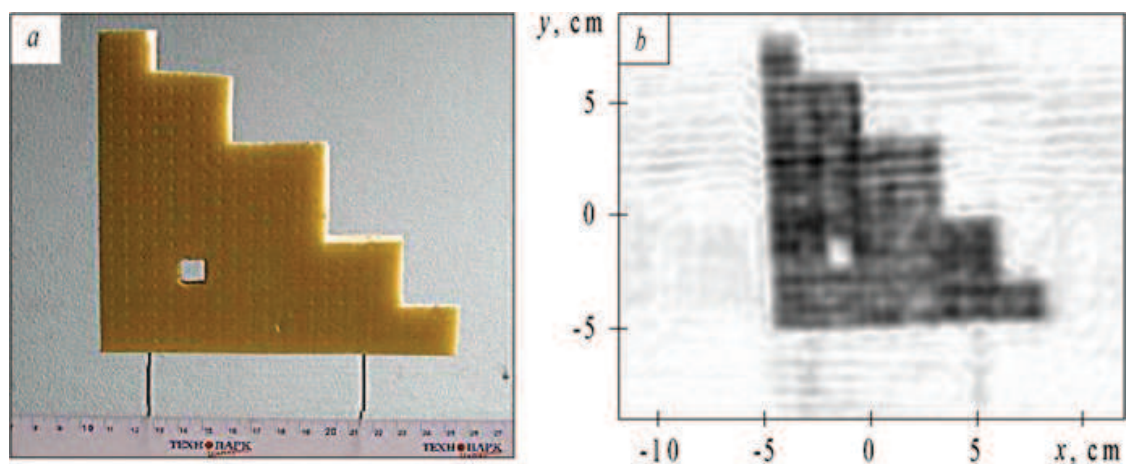


Fig. 8.28 Stepped triangle in air at a distance of 10 cm: (a) photograph and (b) the result of ultrasonic imaging

sounding was performed at all frequencies within the frequency band 37–43 kHz. It should be noted that in air a wavelength of 8.3 mm corresponds to a frequency of 40 kHz, which makes it possible to distinguish fine details in the image.

The resolution of details improves as the distance to the object is decreased. This is because the condition of Fresnel diffraction is being met more precisely (Fig. 8.27).

The reported results confirm the efficacy of the use of ultrasound in location (detection) tomography of small-sized objects. Furthermore, no special permit is required to use ultrasound, so it can be used for covert surveillance.

The result of sounding of a test object in the form of a stepped triangle with a hole is displayed in Fig. 8.28. The resolution in this case is close to the radiating wavelength and even higher.

Objects can be visualized which are hidden behind opaque but acoustically transparent screens (Fig. 8.29). The image is blurred of course, but it remains recognizable. The resolution could be improved significantly with the use of multiple frequencies.

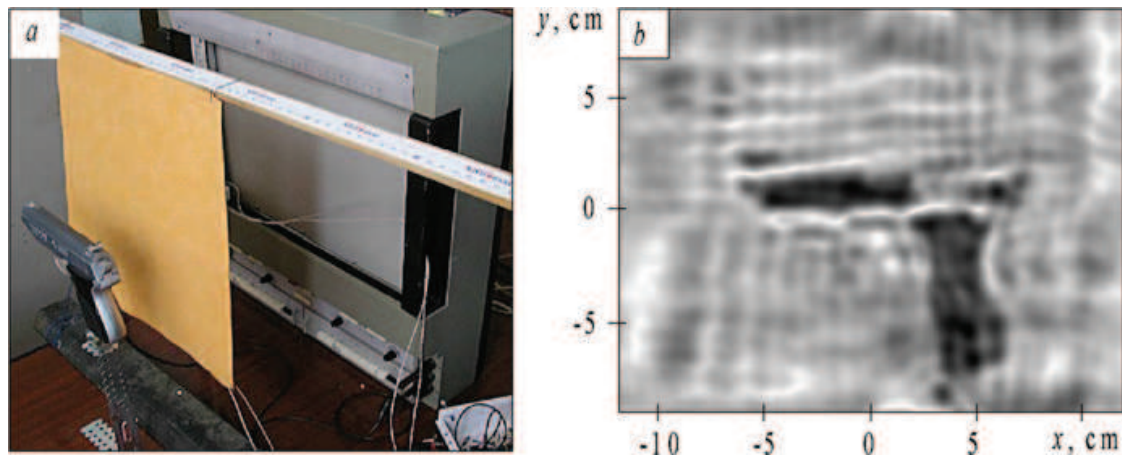


Fig. 8.29 Plastic gun behind a curtain at a distance of 10 cm: (a) photograph of experimental setup and (b) the result of focusing

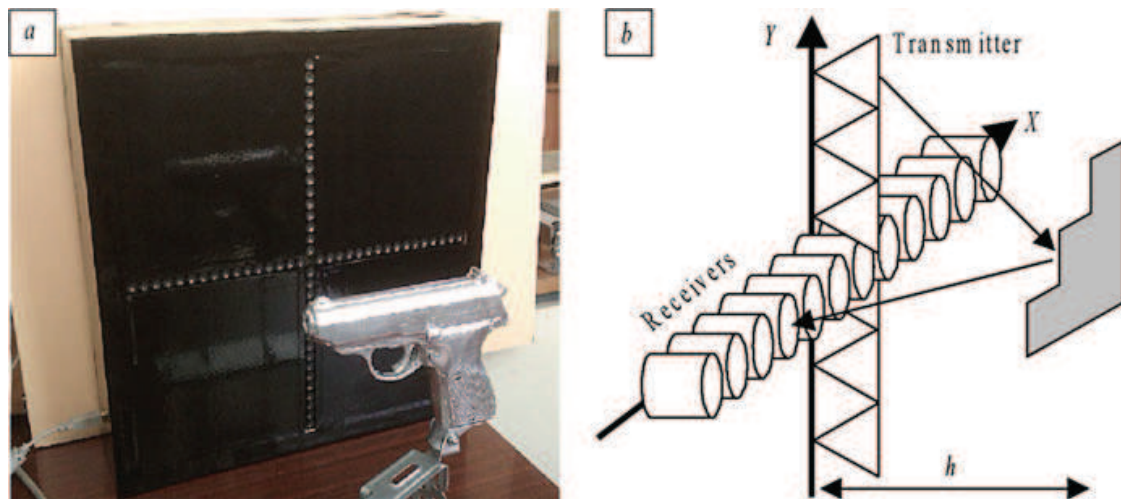


Fig. 8.30 Sonar for contactless ultrasonic imaging: external view (a), configuration scheme (b)

Mechanical scanning of an acoustic field requires up to several tens of minutes, and the object must remain motionless, which is unattainable, e.g., when screening people. Thus, it would be interesting to consider how sounding could be speeded up by electronic switching of the transmit/receive arrays. In the view of the authors, cross-shaped sounding systems are of interest. A demo setup of a sonar was therefore developed that included 32 ultrasonic transmitters and 32 receivers arranged in the form of a cross, situated 1 cm apart from each other (Fig. 8.30).

Measurements were carried out in the clocked mode. The time for a complete measurement, data processing, and visualization of the results on a standard computer does not exceed 2 s, which is acceptable for many applications. An image obtained using the sonar demo setup is presented in Fig. 8.31.

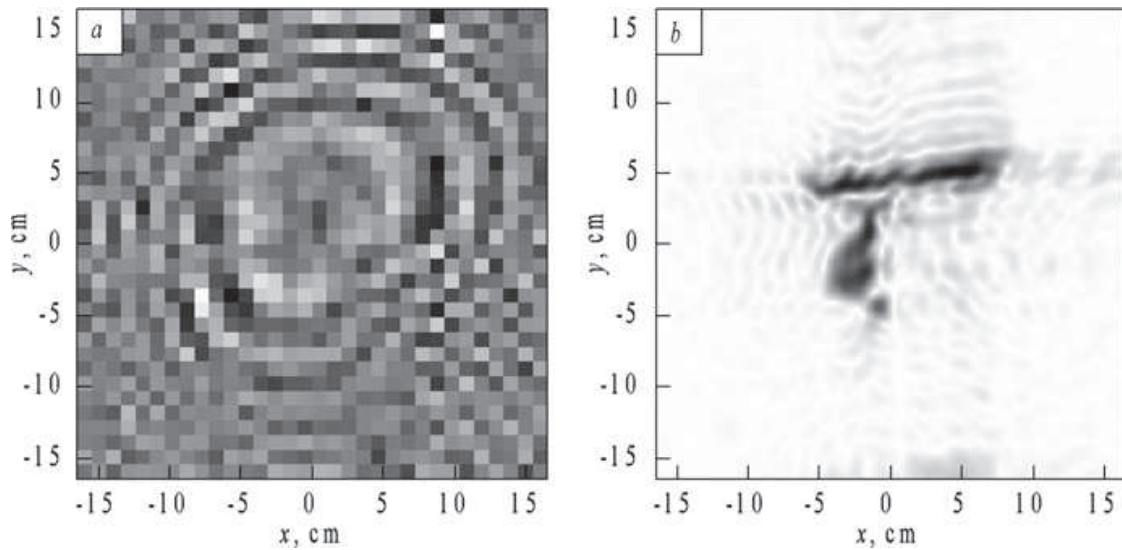


Fig. 8.31 Testing results of sonar demo setup: measured field (a), recovered image (b)

8.3.4 Integration of Radio and Ultrasonic Vision

Ultrasonic radiation mostly is scattered at the inhomogeneities of the density ρ . In remote sounding, it provides the information about the material an inhomogeneity is made of. Using electromagnetic waves in sounding makes it possible to monitor the electrophysical properties of matter. The integration of electromagnetic and acoustic waves for sounding enables us to distinguish solid and liquid media. The following empirical relation is true for solids:

$$\rho = 2(n - 1), \text{ or } n = [\rho/2 + 1],$$

where ρ is the density and $n = \sqrt{\epsilon}$ is the refractive index of the material. A plot of the refractive index versus the density is shown in Fig. 8.32, where the sloped line plots the above dependence.

Note that that TNT, which is distinctly different from other materials, takes a very low position in the diagram. The position of fluoroplastic (Teflon) is close to that of TNT. This means that Teflon can be used to simulate TNT in the laboratory; in real practice, it is necessary to use reconstruction of the shape of such objects to distinguish these materials.

A series of experiments with different objects was carried out (Fig. 8.32). The ultrasound frequency was tuned within the band of 35–45 kHz, and the duration of the UWB pulses was 200 ps. It was established that the images of metallic objects in radio wave tomography have more contrast than in ultrasonic tomography. Apparently, the reason for this is that a part of the energy is spent to excite secondary waves in the metal and behind it.

On the contrary, radio waves have weaker reflection from dielectrics and penetrate into dielectric objects. This was clearly demonstrated in experiments with a metallized grid (the reflection coefficient of radio waves was 0.9, whereas for

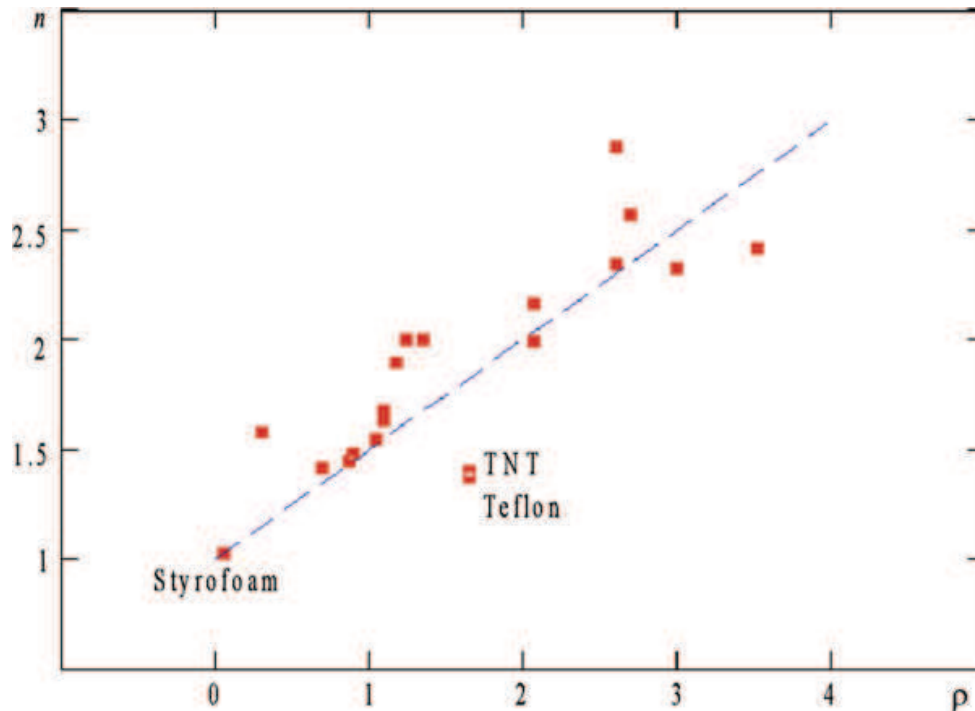


Fig. 8.32 Refractive index – density diagram of several solid materials

ultrasonic waves it was 0.1) and with a foam-plastic object (where the radio waves did not reflect and the reflection coefficient of ultrasound was 0.7). Ultrasound provided higher resolution (of 2–3 mm) than the radio waves (1–2 cm) at identical distances (<1.2 m) to the test object.

The reason for this is the difference between the average operating wavelength for ultrasound (8 mm) and for a radio wave (2 cm). It is important here that the Fresnel zone (the focusing region) for ultrasound has about twice the diameter as for radio waves given the same size of synthetic aperture.

Overlaying the radio wave image and the ultrasonic image of the test object in a false-color combined image makes it possible to judge the material of the test object without additional processing (Fig. 8.33). A similar effect is observed in an element-by-element multiplication of images with a significant increase of the resolution as well.

The combined use of radio waves and ultrasound enables an increase in the information content of the obtained images both in resolution and in the possibility of identifying the material that the sounded object is made of. Radio waves provide penetrating power, for example, under clothing, and ultrasound increases the accuracy of identification of the material of the hidden object. A complete discovery of the possibilities of this approach would require individual study of a wide array of materials using the neural network method.

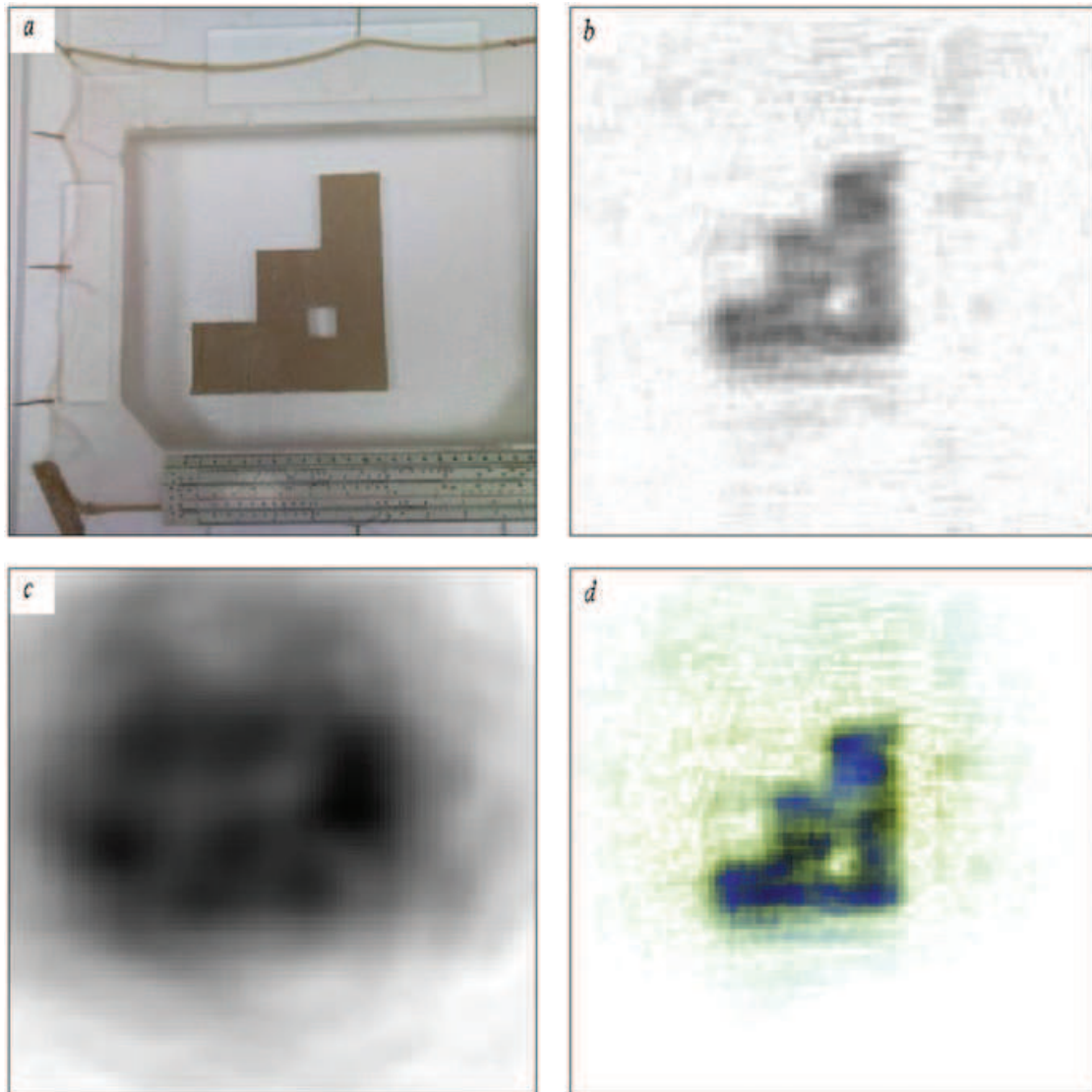


Fig. 8.33 Image of a stepped triangle made of plasterboard behind a metallized grid: (a) photograph, (b) ultrasonic image, (c) UWB image, (d) image from integrated tomography

8.4 Conclusion

Here we have considered new methods of wave tomography. All methods are considered on the basis of a single approach, called tomosynthesis of radio waves. The basis is the idea of creating the effect of focusing radiation waves as a result of interference of a set of partial waves. The connection of the method of wave tomosynthesis with multidimensional sequential filtration and other methods is noted.

A large body of experimental data and their interpretation was obtained within the framework of international collaboration with leading scientists from Magdeburg University (Magdeburg, Germany), the Institute for Non-Destructive Testing (Saarbrücken, Germany), and Tohoku University (Sendai, Japan). I am deeply indebted to Professors A. Omar, M. Kroning, and M. Sato for their collaboration

and also to their colleagues. This text incorporates the most interesting results of other authors but is focused primarily on original in-house research.

I express my special gratitude to my students and coauthors S. Shipilov, D. Sukhanov, A. Klokov, and R. Satarov, as well as the students of my students, who also contributed to the formation of wave tomography. I as the author extend my appreciation to everyone.

References

1. Barrett HH (1982) Optical processing in radon space. *Opt Lett* (7, 6):248–250
2. Baum CE (1973) Introduction to SEM. *IEEE Group Antennas Propagat Int Symp Dig* 11:459–462
3. Baum CE (1986) The singularity expansion method: background and developments. *IEEE Antennas Propagat Soc Newsl* 28(4):14–23
4. Berni AJ (1975) Target identification by natural resonance estimation. *IEEE Trans Aerosp Electron Syst Propagat* 11(2):147–154
5. Chiang B-S et al (1983) Spatial resolution in industrial tomography. *IEEE Trans Nucl Sci* NS-30(2):1671–1676
6. Cordaro JT, Davis WA (1981) Time-domain techniques in the singularity expansion method. *IEEE Trans Antennas Propagat* 29(3):534–538
7. Cormack AM (1963) Representation of a function by its line integrals, with some radiological application. *J Appl Phys* 34(9):2722–2727
8. Moffatt DL, Kennaugh EM (1965) The axial echo area of a perfectly conducting prolate spheroid. *IEEE Trans Antennas Propagat* 13(3):401–409
9. Daniels DJ (1996) *Surface-penetrating radar*. IEE, London, p 300p
10. Dolph CL, Cho SK (1980) On the relationship between the singularity expansion method and the mathematical theory of scattering. *IEEE Trans Antennas Propagat* 28(6):888–897
11. Felsen LB (1985) Comments on early time SEM. *IEEE Trans Antennas Propagat* 33(1):118–119
12. Gaunard GC, Uberall H, Nagl A, Subrahmanyam JV (1982) SEM poles and creeping-wave transients on conductors of simple shapes. *IEEE Int Antennas Propagat Symp* 20:16–17
13. Joaquim F-G (2002) A novel 3-D subsurface radar imaging technique. *IEEE Trans Geosci Remote Sens* 40(2):443–452
14. Kennaugh EM, Cosgriff RL (1958, March). The use of impulse response in electromagnetic scattering problems. *IRE National convention record*, pp. 72–77
15. Marin L (1974) Natural-mode representation of transient scattering from rotationally symmetric bodies. *IEEE Trans Antennas Propagat* 22(2):266–274
16. Mittra R, Pearson LW (1978) A variational method for efficient determination of SEM poles. *IEEE Trans Antennas Propagat* 26(2):354–358
17. Moffatt DL, Mains RK (1975) Detection and discrimination of radar targets. *IEEE Trans Antennas Propagat* 23(3):358–367
18. Mohan R, Rothenberg L, Reinstien L, Ling CC (1995) Imaging in three-dimensional conformal radiation therapy. *Int J Imaging Syst Technol* 6(1):14–32
19. Morgan MA (1984) Singularity expansion representations of fields and currents in transient scattering. *IEEE Trans Antennas Propagat* 32(5):466–473
20. Munk WH (1979) Oceanic acoustic tomography: a scheme for large monitoring. *Deep-Sea Res* 26(2A):123–161
21. Nagl A, Uberall H (1982) Transient radar scattering analyzed in terms of creeping waves. *IEEE Int Antennas Propagat Symp Dig* 20:18–20

22. Pearson LW (1984) A note on the representation of scattered fields as a singularity expansion. *IEEE Trans Antennas Propagat* 32(5):520–524
23. Pearson LW, Roberson DR (1980) The extraction of the singularity expansion description of a scatterer from sampled transient surface current response. *IEEE Trans Antennas Propagat* 28(2):182–190
24. Ramm AG (1980) Theoretical and practical aspects of singularity and cexpansion methods. *IEEE Trans Antennas Propagat* 28(6):897–901
25. Richards MA (1994) SEM representation of the early and late time fields scattered from wire targets. *IEEE Trans Antennas Propagat* 42(4):564–566
26. Sahiner B, Yagle AE (1996) Iterative inversion of the radon transform using image-adaptive wavelet constraints to improve image reconstruction. *IEEE Eng Med Biol* 8(7):395–397
27. Sarkar TK, Weiner DD, Jain VK, Diant SA (1982) Impulse response determination in the time domain – theory. *IEEE Trans Antennas Propagat* 30(4):657–663
28. Stolt RH (1978) Migration by Fourier transform. *Geophysics* 43(1):23–48
29. Swith WE, Barrett HH (1983) Radon transform and band width compression. *Opt Lett* 8(7):395–397
30. Tesche FM (1973) On the analysis of scattering and antenna problems using the singularity expansion technique. *IEEE Trans Antennas Propagat* 21(1):53–62
31. Tseng F, Sarkar TK (1984) Experimental determination of resonant frequencies by transient scattering from conducting spheres and cylinders. *IEEE Trans Antennas Propagat* 32(9):914–918
32. VanBlaricum ML, Mittra R (1975) A technique for extracting the poles and residues of a system directly from its transient response. *IEEE Trans Antennas Propagat* 23(6):777–781
33. Yakubov VP, Shipilov SE, Sukhanov DYa, Klokov AV (2017) Wave tomography. In: Yakubov VP (ed). *Scientific Technology Publishing House, Tomsk*, 248p